Accepted Manuscript

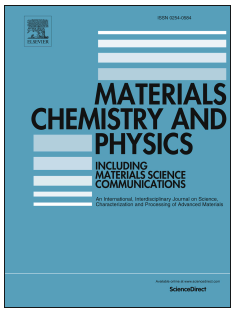

Interrelations of structure, electric surface charge, and hydrophobicity of organo-mica and –montmorillonite, tailored with quaternary or primary amine cations

María del Mar Orta, Federico M. Flores, César Fernández Morantes, Gustavo Curutchet, Rosa M. Torres Sánchez

PII: S0254-0584(18)30948-9

DOI: https://doi.org/10.1016/j.matchemphys.2018.10.059

Reference: MAC 21074

To appear in: *Materials Chemistry and Physics*

Received Date: 1 August 2018

Revised Date: 22 October 2018

Accepted Date: 28 October 2018

Please cite this article as: Marí.del.Mar. Orta, F.M. Flores, Cé.Ferná. Morantes, G. Curutchet, R.M. Torres Sánchez, Interrelations of structure, electric surface charge, and hydrophobicity of organo-mica and –montmorillonite, tailored with quaternary or primary amine cations, *Materials Chemistry and Physics* (2018), doi: https://doi.org/10.1016/j.matchemphys.2018.10.059.

Interrelations of structure, electric surface charge, and hydrophobicity of organo-mica and –montmorillonite, tailored with quaternary or primary amine cations. Pyrimethanil adsorption.

María del Mar Orta[1], Federico M. Flores[2], César Fernández Morantes[2], Gustavo Curutchet[3] and Rosa M. Torres Sánchez[2]*.

[1]*Analytical Chem. Dep. Pharmacy Fac. Sevilla Univ. C/ Profesor García González 2, 41012 Sevilla, Spain.*

[2]*Center for Mineral Resources Technology and Ceramics (CETMIC) - CCT La Plata, CONICET, CICPBA. Camino Centenario y 506, 1897 M. B. Gonnet, Argentine.*

[3]*Environmental Anal. Lab., Environmental Res. and Eng. Institute. National Univ. of San Martin, Av. 25 de Mayo y Francia, San Martin (1650), Argentine.*

Corresponding author. Tel./fax: +54-221-4840247.

E-mail address: rosa.torres@gmail.com; rosats@cetmic.unlp.edu.ar

KEYWORDS: Na-Mica-4, montmorillonite, organo-montmorillonite, organo-mica, octadecyltrimethylammonium, octadecyl-amine.

ABSTRACT

In this work, organo-montmorillonite (organo-Mt) and organo-synthetic mica (organo-mica), obtained by quaternary or primary amine cations (octadecyltrimethylammonium (ODTMA) or octadecyl-amine (ODA), respectively) exchanged at 50% and 100% of their respective CEC, were thoroughly characterized and tested for pyrimethanil uptake. The interlayer entrance of both surfactants for Mt loaded at 50% and 100% CEC indicated a close basal space (of around 1.5 and 1.8 nm, respectively). However, for synthetic mica (Na-Mica-4) the basal space shifted to higher values (3.5 and 3.9 nm and 4.7 and 5.0 nm, for ODTMA and ODA at 50% and 100% CEC, respectively) than those of organo-Mts, keeping the interlayer surface partially free for ODTMA-Mica-4 samples. Tg analysis revealed that the actual ODA loadings were around 40% and 80% for both clays and for ODTMA exchanged Mts, while the actual ODTMA loading for organo-mica samples did not exceed 10.6%. The decrease of negative zeta potential evidenced the presence of ODA or ODTMA at the external surfaces of organo-Mt, while the zeta potential curves

for organo-mica samples described the system as a mixture of individual surfactants and Na-Mica-4 sample. Total specific surface area (TSSA) and contact angle (CA) measurements revealed a general hydrophobicity increment with the presence of both surfactants. Interrelations of these parameters point out the different affinity and steric hindrance of the polar head of both surfactants with the solid surfaces, which also conditioned pyrimethanil adsorption.

1. INTRODUCTION

Mica and montmorillonite (Mt) are 2:1 (tetrahedral-octahedral-tetrahedral) silicates with negative charge coming from different isomorphic substitutions in their structures. These substitutions arises from Si^{4+} exchanged by Al^{3+} in the tetrahedral sheet, while Al^{3+} was exchanged by Mg^{2+} or Fe^{2+} ions in the octahedral sheet. Such negative charge surfaces are balanced by the presence of alkaline or alkaline earth cations (Li^{+}, Na^{+}, K^{+}, Ca^{2+} and/or Mg^{2+}) in the interlayer for Mt and mainly Na^{+} for mica; these coordinated cations between Mt or mica sheets are surrounded by water molecules. Their main properties, such as swelling, cation exchange capacity (CEC) and specific surface area, are related to their chemical composition. Natural micas have no swelling capacity due to the strong electrostatic attraction between layers [1], while the presence of Na^{+} at the Mt interlayer allows it to attain a swelling capacity of more than 35 cc [2]. The synthetic fluorine mica, Na-Mica-4, used in this work has overcome this limitation and swells in water, besides being the most highly charged clay mineral with a cation exchange capacity of up to 4.68 mmol/g [3, 4]. Both the swelling capacity and high CEC properties have determined the applications of Mt and Na-Mica-4, mainly as adsorbents of inorganic cations [5-7] and agricultural pesticides [8, 9].

To enlarge the technological application of clays, one of the strategies used is to tailor the structure by surfactant loading, turning clays into organo-clays.

The replacement of raw Na^{+} and the surface interaction with surfactants such as alkylammonium cations have been proved to protect the mineral structure from acid degradation, causing changes in the interlayer thickness [10, 11],

modifying the electrical charge surface [12], and also the hydrophilic to hydrophobic character [13]. Particularly, changes of electric surface charge generated by surfactant loading modify the coagulation state of the system, driving the aggregation of the particles and the stacking of the surfactant molecules on the surface of the clays [14]. Especially, when the surfactant loading exceeds 100%, of Mt CEC flotation and re-suspension of the system occurs [15].

Notwithstanding the advantages of the organo-clays, it must be taken into account that a different toxicity was assigned to the alkylammonium cations with different chain length, and their release due to the low-strength interaction (hydrophobic) on the outer surface of clays would produce an unwanted contamination. In its application in aqueous effluents, the possible contamination would be reduced by electrostatic attraction with the negative charge colloids present.

Knowledge of the physicochemical properties of organo-clays and the interrelation among them has a major influence on their use in barriers, flammability resistance, biomedical applications, catalytic reactions, adsorption, water treatment, and waste disposal, among others [16-22].

Our recent works evidenced the high potential of organo-Mt [23-25] and organo-micas [26, 27] to adsorb organic pollutants. We mainly used quaternary and primary ammonium cations to synthesize and characterize organo-Mt and organo-mica, respectively. However, to our knowledge, few studies are reported in the literature referring to the interrelation among structure, surface electric charge, and hydrophobicity changes generated by quaternary and primary ammonium cation exchange in synthetic mica and Mt, respectively.

Post-harvest fungicides are applied to fruits to decrease economic losses (usually more than 90% in untreated fruits) caused by fungal decomposition [28]. The use of these products generates large volumes of wastewater with high fungicide concentrations, which are maintained for different periods of time in artificial lagoons to generate maximum aerobic degradation, and reduce environmental pollution. Because the aerobic degradation is not always total and contaminated lagoons are point pollution sources, adsorption treatments can be used to retain the fungicides before their discharge into natural water

sources. Thiabendazole (TBZ) is one of the main fungicides used in fruit production to control mold, blight and other fungi. The resistance to TBZ found in 2004, caused by its intensive use, led to the introduction of new fungicides effective against blue (*Botrytis cinerea*) and gray mold (*Lobesia botrana*) [29, 30]. Pyrimethanil (PRM) is a new fungicide employed to replace TBZ, being one of the most resistant to degradation fungicides used in grapevines [31], although it is classified as a reduced risk fungicide by the US Environmental Protection Agency [32].

The increasing use of PRM has raised concerns about the disposal of agricultural effluents, and the adsorption treatment could allow its removal from contaminated sources.

In this study, the structure, surface charge and hydrophobicity of raw montmorillonite, synthetic Na-Mica-4 and their exchanged products with two loadings of octadecyltrimethyl (ODTMA) or octadecyl (ODA) ammonium are deeply characterized with a combination of techniques, and the results are compared. The knowledge acquired here would help understand the interactions of both organo-clays in order to improve the wide technological applications of these materials. Moreover, the adsorption of pyrimethanil fungicide was particularly evaluated.

2. EXPERIMENTAL SECTION

2.1. Materials

A Patagonian (Rio Negro province) Mt sample, supplied by Castiglioni Pes and Co., was used as received. The main properties of Mt were specific surface area (SSA), 34.0 m^2/g [2]; cation exchange capacity (CEC), 0.83 mmol/g clay; isoelectric point (IEP), 2.7; and apparent diameter (Dapp), 674 ± 51 nm [33]. The XRD analysis of the raw Mt sample indicated that the mineralogical composition was Na-montmorillonite (>99%) with quartz and feldspars as minor phases. The structural formula determined from the chemical analysis of purified Mt was $[(Si_{3.83}Al_{0.11})\ (Al_{1.43}Fe^{3+}_{0.26}Mg_{0.30})\ O_{10}\ (OH)_2]\ Na_{0.30}\ Ca_{0.09}\ K_{0.01}$.[2].

Na-Mica-4 was synthesized by the NaCl melt method following the procedure described by Alba et al. [4]. Briefly, the reactants SiO_2, $Al(OH)_3$, MgF_2, and NaCl were weighed and mixed in an agate mortar until the mixture became homogeneous. They were then heated in a platinum crucible at 900 °C for 15 h at a heating rate of 10 °C/min. The solid was separated by filtration, washed with distilled water, dried at room temperature, and then ground in an agate mortar. The Na-Mica-4 had a SSA of 4.26 m^2/g, CEC of 4.68 mmol/g on an anhydrous basis, and its structural formula was Na_4 $[Si_4Al_4]$ $Mg_6O_{20}F_4$ nH_2O [34].

SiO_2 (CAS no. 112945-52-5, 99.8% purity), $Al(OH)_3$ (CAS no. 21645-51-2), MgF_2 (CAS no. 7783-40-6), and NaCl (CAS no. 7647-14-5, ≥99.5% purity) used for Na-Mica-4 synthesis were purchased from Sigma-Aldrich (Madrid, Spain). Octadecyl-amine (ODA) (CAS no. 124-30-1, ≥99.0% purity), molecular weight (MW) = 269.51 g/mol and critical micelle concentration (CMC), 0.4 mM [35], was also from Sigma Aldrich. Octadecyltrimethylammonium (ODTMA) bromide (≥97%), MW = 392.50 g/mol and CMC, 0.3 mM [36], was supplied by Aldrich Chemical Co. (Milwaukee, WI, USA).

Pyrimethanil (PRM) PESTANAL®, analytical standard (purity 99.9%) was supplied by Fluka-Sigma-Aldrich and used as received. Its physicochemical properties are MW = 199.25 g/mol; solubility in water, 121 mg/L at 25 °C, and pKa = 3.52 (weak base) [37].

2.2. Organic functionalization of Mt and Na-Mica-4 with ODA / ODTMA (organo-Mt and organo-mica)

ODA-Mica-4 and ODA-Mt samples were obtained by a cation-exchange reaction between Na-Mica-4 or Mt and the corresponding amount of ODA to obtain 0.5 and 1 CEC of organo-mica and organo-Mt, respectively. Briefly, the primary amine was dissolved in an equivalent amount of HCl (0.1 M) and the resulting mixture was stirred for 3 h at 80 °C. The alkylammonium solution was then mixed with 10 g/L of Na-Mica-4 or Mt, stirred (200 rpm) for 3 h at 80 ºC, and centrifuged at 8000 rpm. The products were washed three times with distilled water, and finally dried at room temperature and labeled by adding the

theoretical surfactant loading to the name of the absorbent (ODA-Mica-50, ODA-Mica-100, ODA-Mt-50, ODA-Mt-100).

ODTMA-Mt and ODTMA-Mica-4 samples were prepared using the corresponding amount of ODTMA to obtain 0.5 and 1 CEC of Na-Mica-4 or Mt, respectively. The ODTMA solutions were stirred (200 rpm) for 2 h at 60 °C with 10 g/L of Na-Mica-4 or Mt. All products were washed three times with distilled water to remove the counterion excess (tested by $AgNO_3$), lyophilized, and ground manually in an agate mortar. The modified products were labeled ODTMA-Mica-50, ODTMA-Mica-100, ODTMA-Mt-50 and ODTMA-Mt-100.

2.3. Characterization methods

XRD patterns (reflection peak 001) were collected on powder samples over a 2θ range from 1° to 30° with a counting time of 0.1 s/step and 0.03° (2θ) step size, using a Bruker D8 Advance A25 diffractometer (Bruker, Germany) aligned in Bragg-Brentano geometry, operated at 40 kV and 30 mA with Cu K_α radiation.

The average number of clay platelets stacked (n) and its modification by different functionalization were determined as in previous work [38], through the following equation:

$$n = 1 + (D001/d001) \qquad (1)$$

where the mean crystallite domain size, D001, was determined by the Scherrer equation, and d001 was the basal spacing of 001 reflection of the clay layers [39].

Thermogravimetric (Tg) experiments were conducted on the samples using a Rigaku TH 8121-Thermo Plus EVO2 with alumina as a reference. Samples (20 mg) were placed in alumina crucibles and heated from 30 to 1000 °C at a scanning rate of 10 °C/min in air atmosphere. The differential thermogravimetric (DTg) curves were directly derived from the corresponding Tg curves. The actual surfactant loading for all the organically exchanged samples was obtained by calculation from the Tg values in the temperature range from 150 to

800 ºC, or from 170 to 900 ºC, for surfactant loaded Mt or Na-Mica-4 samples, respectively. In organically exchanged Mt the mass loss of Mt structural hydroxyl groups was taken into account [40], while for organically exchanged mica, due to its fluorinate structure, the structural hydroxyl groups were disregarded [34].

Electrokinetic potentials were determined using a Brookhaven 90Plus/Bi-MAS Multi Angle Particle Sizing analyzer (Brookhaven Instruments Corporation, New York, USA) at λ = 635 nm; 15 mW solid state laser; scattering angle, 90º; temperature, 25 ºC, and Pd electrode. The electrophoretic mobility was converted into zeta potential using the Smoluchowski equation [41]. For each determination, 0.05 g of the sample was dispersed in 50 mL of 10^{-3} M KCl solution, and the slurry was stirred. To generate zeta potential versus pH curves, the slurry pH was adjusted using dilute HCl and KOH solutions followed by magnetic stirring until the equilibrium was established (10 min).

The total specific surface area (TSSA) value was determined by water vapor adsorption with relative humidity control (rh = 0.56) as described previously [42].

The particle size distribution was performed in water media on raw Mt and Na-Mica-4 samples employing a Mastersizer 2000 particle size analyzer (Malvern Instruments, UK). The results represented the mean value of nine measurements.

For contact angle (CA) measurements, all samples (0.5 g) were pressed in disc shape of 150 mm diameter using uniaxial pressure (34.3 MPa) and they were sanded to smooth the roughness of the surface. Then, the sessile drop method was used. This method has already been used to evaluate the wettability properties of the surface of micas and montmorillonites [43, 44]. A drop of deionized water (V= 30 μL) was placed on the sample and after 30 ms, when the mechanical perturbations ended, the CA was measured using the photographic camera of the L74PT1600 Linseis thermal microscope at room temperature. The images were analyzed with a plug-in as described by Stalder et al. [45] for the open-source software ImageJ V. 1.46r [46].

2.4. PRM adsorption

The adsorption experiments were carried out in batch conditions, with an adsorbent/adsorbate ratio of 1 g/L using a PRM concentration of 80 mg/L, for 24 h at 20 ºC, under continuous stirring (200 rpm) in Corex glass bottles. A pH of approximately 6.5 remained constant during the adsorption process in all samples. After the contact time, the suspensions were centrifuged at 6,000 rpm for 15 min. The concentration of PRM in the supernatants was analyzed by high performance liquid chromatography (HPLC) coupled with UV-visible detection (λ = 270 nm) using a Shimadzu HPLC C18 column (4.6 mm × 250 mm, 4.6 μm). The mobile phase was a 70/30 acetonitrile/water mixture flowing at 1 mL/min. The volume injected in the chromatography system was 20 μL. The presence of different amounts of surfactants was checked so they did not interfere with the PRM determination. The amount of adsorbed PRM, *q* (μmol PRM/g clay), was determined as the difference between the initial PRM concentration (C_i) and the concentration after contact time (C_e).

The adsorption percentage was calculated by the following expression:

$$\%\text{adsorption} = (C_i - C_e) / C_i \times 100\% \qquad (2)$$

3. RESULTS

3.1. XRD patterns

The shift of the basal reflection allows following the incorporation of surfactant into the interlayer of the Mt or Na-Mica-4 samples. Fig. 1A and B show the XRD patterns of Mt and Na-Mica-4 (and their respective organo-Mt and -Mica-4 products), respectively.

The 001 value found for the Mt sample (Fig. 1A) was 1.26 nm with a shoulder at 1.43 nm. The structural formula of Mt indicated that Na^+ and Ca^{2+} were the main cations present in the interlayer. The 001 peak deconvolution (Fig. S1 in the Supplementary material), with an R^2 fit of 0.996, corresponds to the existence of ~~a~~n heterogeneous interlayer resulting from the presence of Na^+ and Ca^{2+} [47]. The ratio of the areas, within the peak 001, Na/Ca = 1.18, was related to the greater presence of Na^+ than Ca^{2+}, as indicated by the structural formula.

For Mt, the 001 value shift from 1.26 nm (Fig. 1A) to higher values depended on the amount and type of surfactant loaded (ODTMA or ODA). The interlayer space of ODTMA-Mt and ODA-Mt samples was determined by subtracting the space of dehydrated Mt (0.97 nm) from the 001 value.

The calculated interlayer spaces for ODTMA-Mt samples were 0.46 and 0.88 nm, for 50% and 100% CEC, respectively. The values found for ODTMA-Mt-50 and ODTMA-Mt-100 samples were consistent with previous data [12] and indicate a lateral monolayer and pseudo-trilayer or a paraffin-like monomolecular arrangement of the surfactant, respectively [48]. Particularly, in the ODTMA-Mt-50 sample, the 001 peak deconvolution (inset in Fig. 1A) indicated the existence of two overlapping peaks at 1.43 and 1.64 nm, which correspond to a transition of surfactant arrangement with an interlayer increase of 0.46 and 0.67 nm, respectively, with an R^2 of 0.996, and a ratio area of 1.26 [11]. Furthermore, in hexadecyltrimethylammonium exchanged Mt, XPS measurements showed a complete replacement of the original Na^+ cations and only one third of the original Ca^{2+} [49]. The presence of this hydrated remnant Ca^{2+} and the lateral monolayer arrangement of ODTMA explain the increase of the interlayer space found in ODTMA-Mt-50 sample.

For ODA-Mt samples, the interlayer space was 0.53 and 0.79 nm for ODA-Mt-50 and ODA-Mt-100 samples, respectively [16]. Additionally, as in ODTMA-Mt-50, in ODA-Mt-50 sample the 001 peak deconvolution (inset in Fig. 1A) indicated the existence of two peaks at 1.61 and 1.43 nm, with an R^2 of 0.997, and a ratio area of 1.33. This behavior could be explained by the interlayer heterogeneity, generated by the ODA arrangement similar to that of ODTMA, and the presence of some remnant hydrated Ca^{2+}. Despite the similar arrangement found for both surfactants, it was evidenced that the exchange with quaternary amine cations caused a greater expansion of the interlayer space than the primary ones, which would be related to the larger size of the quaternary amine heads.

The average number of platelets stacked with high crystalline order, n, determined by eq. 1, provided an unambiguous indication of the stacking order of the clay platelets. The n values obtained were: 8.8, 12.8, 9.8, 11.8 and 10.7 for Mt, ODTMA-Mt-50, ODTMA-Mt-100, ODA-Mt-50 and ODA-Mt-100 samples,

respectively. The increase of n value at both low surfactant loadings (0.5 CEC) and further decreases at larger loadings agree with data of previous work [38, 39], for hexadecyltrimethylammonium loaded Mt samples. Huang et al. 2017 [39] explained the increase in the average number of platelets stacked at low surfactant loading by a bridging interaction of the organic cations between different basal clay planes, producing an interconnection when the monolayer is formed. While at higher surfactant loading, the larger interlamellar distances generated by pseudo-trilayer or paraffin-like monomolecular layers introduce disorder in the stacking direction of the layers, decreasing the average number of stacked platelets. These behaviors reflected significant structural changes in the organo-clays whichever quaternary or primary amine cations were loaded.

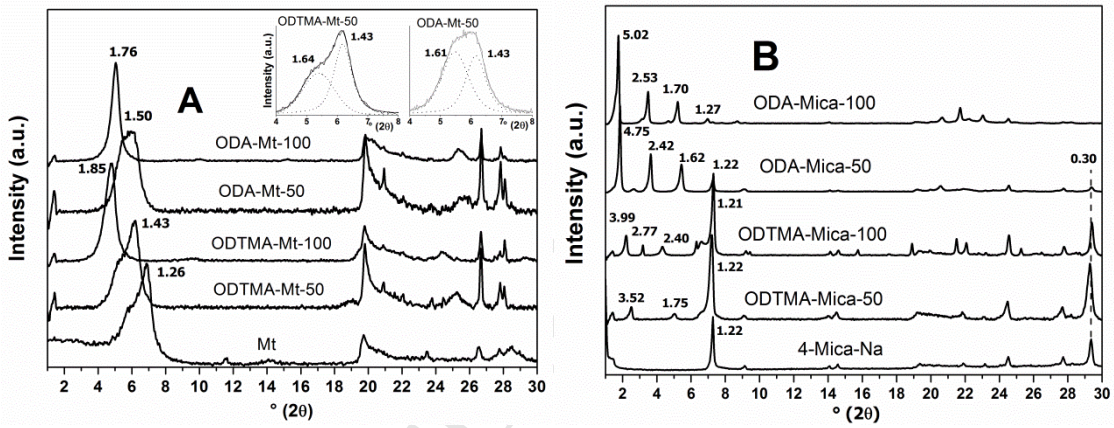

Fig. 1. XRD patterns of (A) Mt and (B) Na-Mica-4 and the respective ODA / ODTMA loaded samples. Insets: deconvolution of 001 peak for indicated samples.

The basal space of Na-Mica-4 sample at 1.22 nm and the well-ordered sequence of the 00l reflection [50] are shown in Fig. 1B.

In ODTMA loaded Na-Mica-4 at 50% and 100% CEC, the basal space at 1.22 nm [50] remained unchanged, and several higher-order peaks were observed at lower 2θ in Fig. 1B (1.75 and 3.52 nm, and 2.40 and 2.77 nm for ODTMA-Mica-50 and ODTMA-Mica-100 samples, respectively), whose intensities seem to increase with the amount of ODTMA exchanged. As explained above for ODTMA-Mt, a heterogeneous interlayer space results from the different arrangements or random orientation of ODTMA [48]. Particularly, the peak at 3.99 nm in ODTMA-Mica-100 sample was related to the presence of

a superstructure of ionic pairs ($ODTMA^+$ Br^-) [48]. However, Tamura and Nakazawa [51] assigned this interlayer spacing to a paraffin-like arrangement of the surfactant. Furthermore, for ODTMA-Mica-50 and ODTMA-Mica-100 samples, the 004 peak at 0.30 nm indicated that the interlayer space remained partially free of ODTMA. The presence of Na^+ ions remaining at the interlayer in ODTMA-Mica samples was evidenced by the high intensity of 1.22 and 0.30 nm peaks, which was in agreement with recent results [52], indicating a great difficulty in achieving complete intercalation [53] and leading to the formation of a product that combines the functionality of a surfactant with the structural properties of the inorganic component.

For ODA modified Na-Mica-4 samples, the well-ordered sequence of the 00l reflection is in agreement with Pazos et al. [50]. The peak at 1.22 nm of Na-Mica-4 is assigned to the presence of Na^+ in the interlayer; the ODA by Na^+ exchange decreases the intensity of this peak in ODA-Mica-50 and -100 samples with respect to Na-Mica-4. The basal space at 4.75 and 5.02 nm for ODA-Mica-50 and ODA-Mica-100 samples, respectively, which indicated an interlayer increase of 3.78 and 4.05 nm, respectively, also corresponds to a paraffin-like arrangement of the surfactant (>2.20 nm) [12].

The comparison of the peak intensity of 1.22 nm between mica samples exchanged with ODA or ODTMA would indicate a different amount of surfactant exchanged, as will be determined in the next section. In addition, these results suggest a greater affinity of the mica surface with the primary amine cations with respect to the quaternary ones, contrary to that found for Mt sample.

For Na-Mica-4 and its products loaded with surfactant, the average number of platelets stacked with high crystalline order, *n*, could not be determined due to the large errors generated by the closeness of the low full width at half maximum of the reflection peak with the instrumental width.

3.2. Thermogravimetric analysis

Thermogravimetric analysis was used to confirm clay modification by surfactant loading and to determine the actual % CEC.

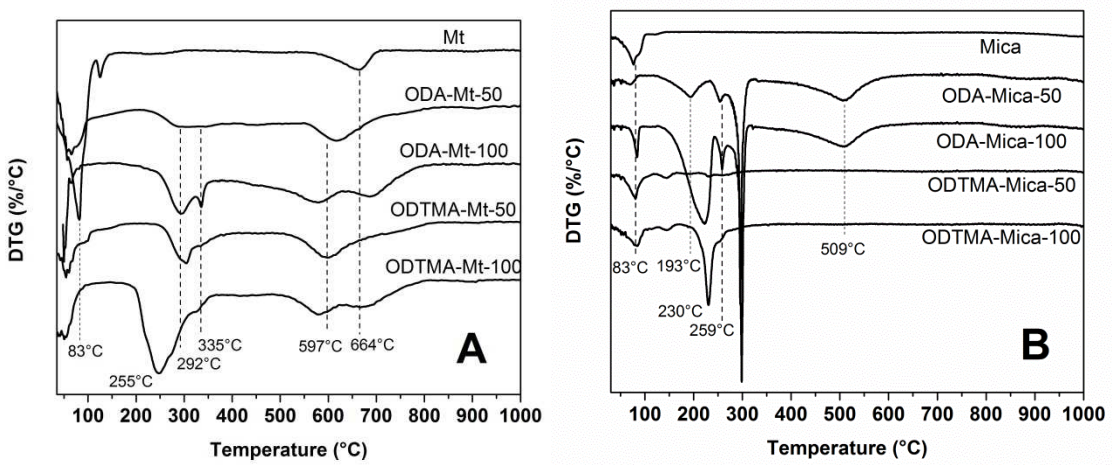

Fig. 2. Derivative plot of thermal degradation (DTg) for A) Mt and ODTMA / ODA loaded Mt samples, and B) Na-Mica-4 and ODTMA / ODA loaded mica samples.

The thermal decomposition of Mt was analyzed in three temperature ranges, while for its surfactant loaded forms four temperature ranges were needed in order to take into account different interactions or association mechanisms between the clay and the surfactant (Fig. 2A) [54].

Table 1. Percentage of mass loss in Mt and organo-Mt and actual surfactant loaded with respect to the % CEC Mt. The mass loss of net ODTMA was added in order to evidence its full combustion up to 800 °C.

Sample	% mass loss				% CEC loaded
	25-150 (ºC)	150-300 (ºC)	300-550 (ºC)	550-800 (ºC)	
ODTMA	1.2	78.4	12.3	2.8	
	Loss of water	Van der Waals	Cation Exchange	Dehydroxylation layered silicate	
Mt	14.3	1.0	0.9	3.0	-
ODTMA-Mt-50	5.9	2.5	6.5	7.9	40.6
ODTMA-Mt-100	4.0	10.5	8.6	9.5	88.0
ODA-Mt- 50	4.6	2.2	6.3	8.9	47.5
ODA-Mt-100	1.7	3.3	10.5	10.6	76.4

For Mt sample a 14.3% mass loss at temperature < 150 °C was attributed to the loss of physically adsorbed water (Table 1). The 150 to 550 °C range assigned to surfactant decomposition showed a low mass loss [54, 55]. In the 550 and 800 °C range, a mass loss of 3.0% represented by a DTg peak at 664 °C was assigned to the loss of structural hydroxyl groups.

Loading of Mt samples with ODTMA produced a decrease in the mass loss of water at temperature <150 °C with respect to that found in Mt sample (Table 1). This effect was mainly associated with Na^+ and its hydration sphere exchange with $ODTMA^+$ within the interlayer (Fig. 1 A), with the subsequent decrease of the DTg peak with respect to that of Mt at 83 °C (Fig. 2A). In the 150-800 °C range, an increase in mass loss was observed compared to that of Mt sample (Table 1), giving an actual ODTMA loading of 40.6% and 88.0% CEC in ODTMA-Mt-50 and ODTMA-Mt-100 samples, respectively. These data were consistent with those found in previous work [33]. This temperature range was divided into two new ranges (from 150 to 300 and from 300 to 550 °C, Tables 1 and 2), assigned to Van der Waals and cation exchange interactions between Mt and the surfactant (Fig. 2A) [11]. In the ODTMA-Mt-50 sample, the cation exchange of ODTMA within the Mt interlayer sites generated a peak at around 305 °C, with a mass loss of 6.5 % (Table 1). Particularly, for ODTMA-Mt-100 sample, the cation exchange mechanism created a shoulder at around 305 °C, and the van der Waals interactions produced a peak at 255 °C (Fig. 2A) [11], with a mass loss of 8.5% and 10.5%, respectively (Table 1). The general decrease in thermal stability of ODTMA exchanged Mt samples that occurs when the surfactant loading increase is in agreement with previous work [33].

In the third step of decomposition (550-800 ºC), there was a shift of the DTg peak of Mt (664 ºC) to lower temperatures (around 580-597 °C), which was attributed to the surfactant penetration into the ditrigonal cavity of the clay [56]. Besides, a last organic matter oxidation step occurred at 677 °C in ODTMA-Mt-100 sample [56].

For ODA-Mt the DTg curve observed was similar to that of ODTMA-Mt, at the first temperature range (<120 °C) (Fig. 2A). However, while the mass loss in ODA-Mt-50 and ODTMA-Mt-50 samples was similar, a lower mass loss was found in ODA-Mt-100 with respect to ODTMA-Mt-100 samples (Table 1). This

indicates a lower water replacement from the interlayer or physisorbed in the former sample. The calculated CEC loaded was 47.5% and 76.4% for ODA-Mt-50 and ODA-Mt-100 respectively (Table 1). In ODA-Mt-50 and -100 sample the DTg peaks assigned to van der Waals and cation exchange interactions appeared at higher temperature (292 and 335 °C, respectively) than those found for ODTMA-Mt samples, indicating stronger interactions within ODA and the Mt surface. Le Pluart et al. [57] assigned the appearance of a DTg peak at around 250 °C to n-octylamine ions physisorbed on Mt, which were completely removed by water washing, while the washing did not remove the ionically bonded ions in the interlayer. This behavior is in agreement with the results of Cowan and White [58], who measured the free energy values of ion exchange for primary amines adsorbed on Mt and reported that the adsorptive forces are overcome by the solvating effect of the water molecules. The presence of n-octylamine ions physisorbed on Mt could overestimate the calculation of the % of the CEC exchanged with ODA surfactant (Table 1). In this work, both ODA-Mica and ODA-Mt samples were washed only with water to achieve a better comparison between these samples, because washing of Mt with alcohols also produces its interlayer intercalation and a reduction in the interlayer space [24, 59].

At the highest temperature range (550-800 °C), the ODA loaded Mt samples showed a mass loss and DTg peaks similar to those of ODTMA loaded Mt samples.

The thermal decomposition of Na-Mica-4 and its organo-mica products (Fig. 2B) was analyzed in almost the same temperature ranges as those for Mt and organo-Mt samples, which correspond to water loss and surfactant decomposition, respectively [60]. The DTg of Na-Mica-4 showed a mass loss of 5.3% (Table 2) attributed to the water molecules released from the interlayer space, which produced a DTg peak at 83 °C (Fig. 2B).

Table 2. Percentage of mass loss in Na-Mica-4 and organo-micas and actual surfactant loaded with respect to the % CEC of Na-Mica-4.

Sample	% mass loss	% CEC

	25-120 (ºC)	120-270 (ºC)	270-400 (ºC)	400-800 (ºC)	loaded
ODA	2.7	45.4	51.1	0.5	-
	Loss of water	Van der Waals	Cation Exchange	Dehydroxylation layered silicate	
Na-Mica-4	5.3	0.1	0.1	1.0	-
ODTMA-Mica-50	5.9	2.9	0.9	2.1	2.6
ODTMA-Mica-100	5.6	11.0	1.9	1.7	10.6
ODA-Mica-50	2.2	9.1	14.2	13.8	43.1
ODA-Mica-100	3.1	28.6	13.8	12.3	88.6

For ODTMA loaded Na-Mica-4, at the lower temperature range (<120 °C), the mass loss (Table 2) and DTg peak remained similar to those found for the Na-Mica-4 sample, irrespective of the surfactant amount loaded.

The 120-900 °C range was used to calculate the actual ODTMA-Mica loaded samples, being of 2.6 and 10.6% CEC exchanged for ODTMA-Mica-50 and ODTMA-Mica-100 samples, respectively (Table 2). The low surfactant exchange in ODTMA-Mica-50 sample, due to its difficulty to attain a complete intercalation [53], was confirmed by the presence of a 004 peak, indicative of a main interlayer space free of surfactant (Fig. 1B) or incomplete Na^+ replacement by the organic ions at the interlayer of the synthetic mica, and formation of ionic pairs as indicated by XRD (Fig. 1B).

The DTg peaks at 230 and 259 °C present in ODTMA-Mica-100 sample could be attributed to surfactant molecules weakly adsorbed on the clay surface by van der Waals interactions, or ionic pairs as indicated in Section 3.1.

The steric effects of the quaternary amine cations in ODTMA-Mica-100 and ODTMA-Mica-50 samples pose a greater difficulty that prevents the coexistence of organic and inorganic species [52], leading to the low amount of ODTMA loaded (Table 2).

The mass loss, within 120 and 900 °C, determined for ODA-Mica samples (Table 2) was higher than that of ODA-Mt samples (Table 1).However, the actual % CEC values obtained were similar due to the different CEC values of

both Na-Mica-4 and Mt samples. Additionally, the presence of physisorbed ODA in mica samples could overestimate the calculation of % CEC loaded values.

For ODA loaded mica samples, at the lower temperature range (<120 °C), the DTg peak for water loss remained at the same temperature, with a mass loss slightly lower than that found for Na-Mica-4, indicating that the mass loss was not related to the ODA amount loaded. From 120 to 900 °C five DTg peaks at 193, 230, 259, 300 and 509 °C were found. The peak at 193 °C in ODA-Mica-50 and also that at 230 °C in ODA-Mica-100 sample can be assigned to physisorbed ODA as ionic pairs, as in ODA-Mt samples (at 292 °C). The DTg peaks at 259 and 300 °C were related to the simultaneous presence of alkylammonium ions as ionic pairs and exchanged, respectively, in both ODA-Mica-50 and ODA-Mica-100 samples [50]. The DTg peak at 509 °C could be attributed to residual charcoal from organic matter oxidation [61].

The cation exchange decrease from 88.6% CEC (ODA-Mica-100) to 43.1% CEC (ODA-Mica-50) shown in Table 2 was in agreement with the higher Na^+ exchange obtained for ODA-Mica-100 than for ODA-Mica-50 identified by XRD analysis. This higher amount of Na^+ exchanged by ODA in ODA-Mica-100 than in ODA-Mica-50 samples generated the intensity decrease of the peak at 1.22 nm in both samples.

3.3. Zeta potential data

The electrical charge surface measured by the micro-electrophoresis method allows evaluating the electrical surface charge changes at the external surface produced by the surfactant loading, because the neutral constancy of the interlayer remains with the cation exchange [62]. Fig. 3 (A to D) shows zeta potential vs. pH curves for Mt, Na-Mica-4 and the respective ODTMA / ODA loaded samples.

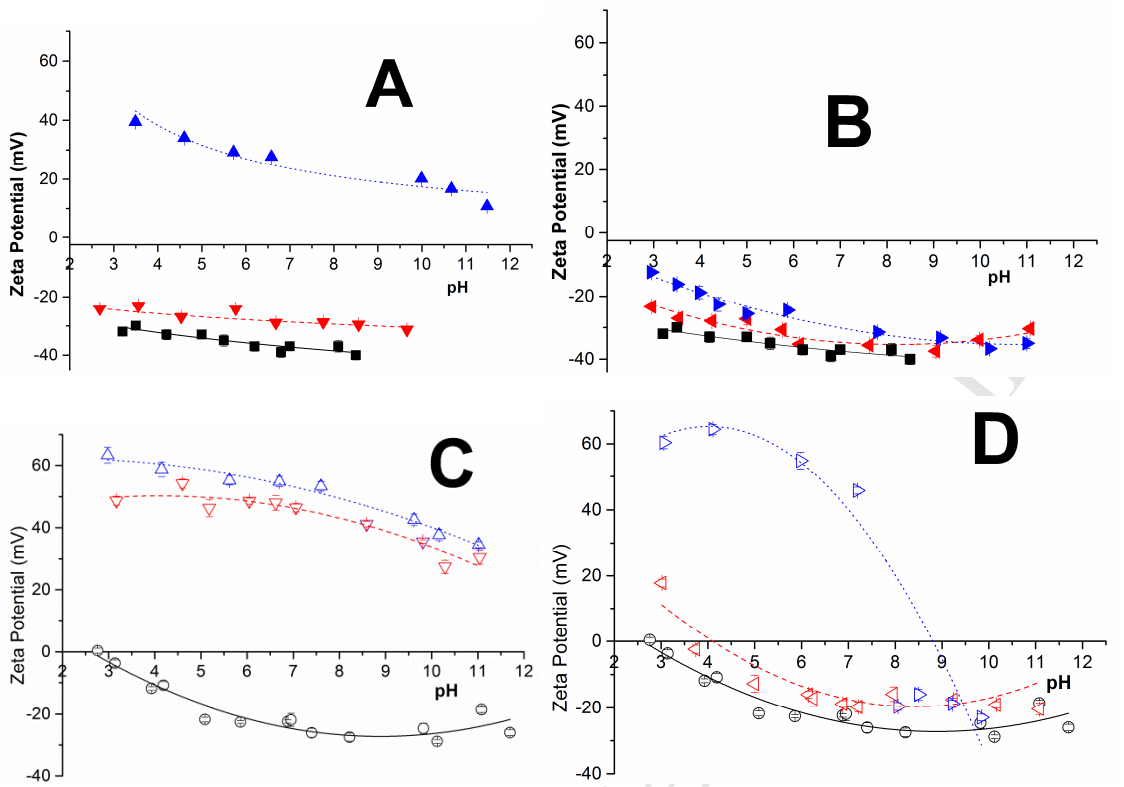

Fig. 3. Zeta potential versus pH curves for (A) (■) Mt, (▼) ODTMA-Mt-50 and (▲) ODTMA-Mt-100; (B) (■) Mt, (◀) ODA-Mt-50, (▶) and ODA-Mt-100; (C) (○) Na-Mica-4, (▽) ODTMA-Mica-50, and (△) ODTMA-Mica-100; and (D) (○) Na-Mica-4, (◁) ODA- Mica-50, and (▷)ODA-Mica-100 samples.

The pH-independent zeta potential behavior (at around -30 mV) over the entire pH range (from pH 3 to 10) for Mt sample (Fig. 3A and B) is produced by a constant surface potential (structural or basal sites) and variable charge (edge sites). The flat curve found for Mt sample is similar to that previously published [63].

ODTMA loading on Mt (Fig. 3A) produced a decrease in the raw negative surface electric charge of about 10 mV in ODTMA-Mt-50 sample and a reversal to positive surface electric charge in ODTMA-Mt-100 sample [12]. The electric charge behavior of the latter sample was due to an external surface coverage increase [64] and the ammonium group arrangement in head to tail orientation [65].

After ODA loading on Mt (Fig. 3B) the actual surfactant amounts were close to those of ODTMA (Table 1); however, only a slight decrease of negative

surface electric charge was attained with respect to that of Mt sample. In order to explain this behavior, two effects must be taken into account. First, due to the smaller size of the ammonium head groups in the ODA ($-NH_3^+$) compared to the ODTMA [$-N(CH_3)_3^+$] surfactant, when their concentrations increase the former can be arranged mostly perpendicularly to the surface [66], decreasing the initial negative surface charge and without electric charge investment. However, the steric hindrance of ammonium head groups of ODTMA generated a head-tail orientation on the surface, which exposed the positive head groups, and consequently the negative surface electric charge was reversed (Fig. 3A). The second effect, as reported by Wang et al. [67], was assigned to the possibility of primary ammonium head groups to generate additional hydrogen bonds with water molecules and chloride anions onto clay surfaces, and consequently if a positive surface charge is generated, it would be almost neutralized [66, 67].

The negative zeta potential, from 0 to -30 mV at the pH range studied, obtained for Na-Mica-4 (Fig. 3C and D) was in agreement with data found for raw mica [68].

ODTMA loading of Na-Mica-4 produced a complete reversal of the initial negative to high positive electric charge values (Fig. 3C). Taking into account that the XRD analysis indicated that the surface of the interlayer remained partially free of ODTMA, the positive electric charge observed in both ODTMA-Mica samples, despite their low % of CEC exchanged, could be assigned to ODTMA loading occurring mainly on Na-Mica-4 external surface. However, the high positive zeta potential values obtained (around 50 mV) for both samples cannot be correlated, as in ODTMA-Mt-100 sample, with the amount of surfactant exchanged (Table 2). This behavior could be explained by the presence of ODTMA as free ionic pairs of the Na-Mica-4 surface acting as a mixture with the latter. This demeanor has been previously described in mixtures of soil components [69], where another electric charge parameter, such as the point of zero charge (PZC) of the mixture, was related to the surface provided by each component and their individual PZC [70]. In order to determine the presence of an arrangement as a mixture of the components of ODTMA-Mica samples, a mechanical mixture of Na-Mica-4 and solid ODTMABr (ratio 40:7 w/w), corresponding to the same amounts by weight of the sample

ODTMA-Mica-100, was evaluated by zeta potential measurements. Since 10% CEC ODTMABr solution corresponds to a concentration = 0.47 mM ODTMABr, which is higher than its CMC (0.3 mM), micelles can be formed. The zeta potential value of an ODTMABr suspension with a concentration higher than its CMC was also measured check for the micelle formation. The zeta potential value of ODTMABr solution reached 70 mV, and the zeta potential curve obtained for the Na-Mica-4/ODTMA mixture (Fig. S2 in the Supplementary material) was close to that of ODTMA-Mica-50 and ODTMA-Mica-100 samples. According to these observations, it can be suggested that the positive zeta potential in ODTMA-Mica-50 and ODTMA-Mica-100 samples was generated by their suspensions acting like mixtures of Na-Mica-4 and surfactant components, the latter released from the surface to the solution.

For Na-Mica-4 loading with ODA, the electric charge reversal only occurred in ODA-Mica-100 sample, which has a loading percentage close to the CEC of Na-Mica-4 (Table 2). This behavior could be attributed to the release of ODA to the solution at low pH, because of the high solubility and stability of the primary alkylammonium cations in acid solutions [36]. This electric charge reversal was not seen in ODA-Mt-100 sample, and was assigned to the presence of stronger interactions between ODA and the surface of Mt than with the surface of Na-Mica-4. This behavior was corroborated by a DTg peak at higher temperature for the former surface (Fig. 2A). Particularly, in the zeta potential curve of ODA-Mica-50 sample, due to its low ODA loading, the electric charge inversion was not observed, except at acid pH in agreement with the behavior mentioned previously.

3.4. Total specific surface area and hydrophobicity

As described in a previous study [23], an underestimation of the SSA of swelling clays may occur when nitrogen is used as a probe molecule due to specific interactions between nitrogen and the polar interlayer surface sites [23]. Consequently, the use of nitrogen only allows the determination of the external specific surface area (ESSA) of the clay [71], which accounts for up to 10% of the total specific surface area (TSSA) depending on the particle size and mainly

on the amount of stacked sheets of the tactoids formed [23]. In contrast, the use of water vapor as probe molecule allows the determination of the TSSA as a sum of the inner (interlayer) surface and the external one [23]. It should be noted that for comparative purposes, the determination of TSSA by water adsorption must be carried out under conditions of similar initial degassing, constant rh = 56% during equilibration and taking into account that the residual water content strongly depends on the inorganic cation present in the interlayer of the raw clay [72].

Table 3. TSSA and CA values of raw Na-Mica-4, Mt and their ODTMA / ODA loaded samples.

Sample	TSSA (m^2/g)	CA (°)
Mt	358 ± 6	57 ± 5
ODTMA-Mt-50	125 ± 4	76 ± 2
ODTMA-Mt-100	84 ± 2	80 ± 3
ODA-Mt- 50	185 ± 2	106 ± 3
ODA-Mt-100	49 ± 8	96 ± 2
Na-Mica-4	202 ± 10	33 ± 2
ODTMA-Mica-50	169 ± 9	51 ± 1
ODTMA-Mica-100	159 ± 2	52 ± 3
ODA-Mica-50	74 ± 7	110 ± 2
ODA-Mica-100	58 ± 1	99 ± 1

The sum behavior of TSSA value is evidenced by the values of 202 and 358 m^2/g obtained for Na-Mica-4 and Mt, respectively (Table 3), compared to the lower SSA values of 4.3 and 34.0 m^2/g attained for the same samples, respectively. It is worth noting that the SEM analyses of Na-Mica-4 and Mt samples published previously [73, 74], respectively, indicate hexagonal morphology and curved plates with face-to-edge contacts between particles, respectively, with estimated particle sizes from 2 to 10 μm and from around 1 μm, respectively, which are in line with the decrease in both surface area values. In order to corroborate the particle size values obtained by SEM

observation elsewhere, determinations of particle size distribution values were performed in this work (Fig. S3, in the Supplementary material). The Na-Mica-4 sample showed a bimodal distribution with D_{50} = 96.4 μm, while for Mt sample a trimodal distribution was found with D_{50} = 7.1 μm. Both D_{50} values obtained, despite the morphology differences within Mt and Na-Mica-4 samples, point to a lower specific surface value for the latter sample, in agreement with Table 3 results.

The occupancy of the organo-clay surface by surfactants produced a general decrease in the TSSA values by the interlayer occupancy indicated by XRD measurements, compared to the corresponding raw clay, and irrespective of the surfactant used (Table 3).

However, the variation in TSSA values with the loading increase in ODTMA and ODA in Mt or Na-Mica-4 samples (Tables 1 and 2, respectively) indicated a different behavior of each surfactant.

In order to evaluate the hydrophilicity/hydrophobicity changes of ODA and ODTMA loaded samples, the TSSA, CA (Table 3) and the % CEC values (Tables 1 and 2) were 3 D plotted (Fig. 4). TSSA, CA values and % CEC= 0 for Mt and Na-Mica-4 samples were also added for comparison purposes. The accuracy of the method used to determine CA in this work was verified by the CA value of 57º obtained for Mt (Table 3) that is close to that reported for a reference Mt and obtained with a commercial CA microscope [49].

The general increase in CA values with ODTMA and ODA loadings (Table 3) confirms the increased hydrophobic property with respect to the hydrophilic surface of Mt and Na-Mica-4 samples.

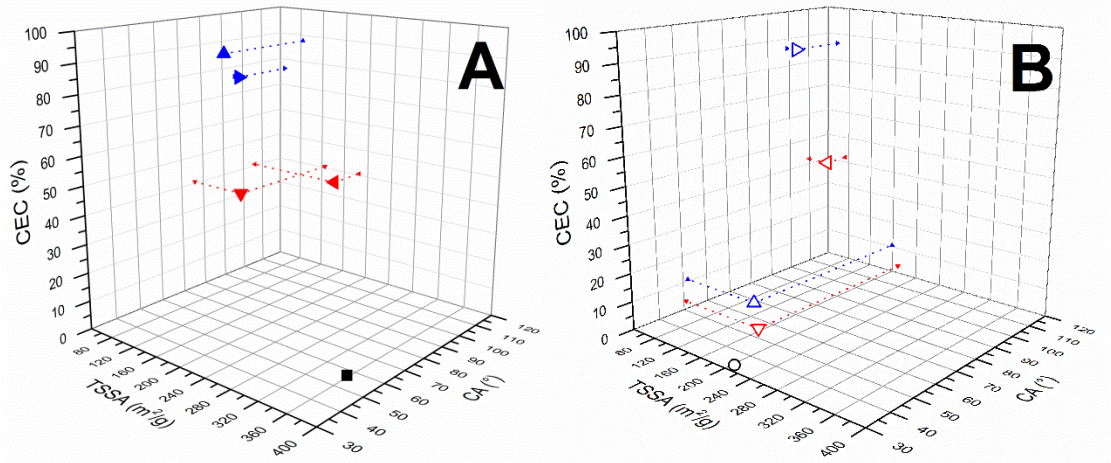

Fig. 4. 3D plot of % CEC, TSSA and CA values for .(A) (■) Mt, (▼) ODTMA-Mt-50 and (▲) ODTMA-Mt-100, (◀) ODA-Mt-50, (▶) and ODA-Mt-100; (B) (○) Na-Mica-4, (▽) ODTMA-Mica-50, and (△) ODTMA-Mica-100, (◁) ODA- Mica-50, and (▷)ODA-Mica-100 samples. The CEC value of raw samples (Mt and Na-Mica-4 samples) was taken as zero in order to compare TSSA and CA values with the % CEC increase of the respective surfactant loaded. The dotted lines indicate the point projections to the ZX and ZY planes.

The CA values were higher for ODA than for ODTMA loaded samples. This effect can be associated with the orientation of both molecules on the surface. As mentioned above, the polar group of some ODTMA molecules could not be in contact with the surfaces due to the steric hindrance (head-tail arrangement orientation), while the ODA molecules make that surface contact (arrangement of the hydrophobic tail opposite the surface).

For ODTMA loaded Mt samples, a decrease and an increase of the TSSA and CA values, respectively, with the surfactant content was observed (Fig. 4A). However, for ODTMA loaded Na-Mica-4 samples (Fig. 4B), while the TSSA values decreased, the CA values remained almost constant. Roughly, ODTMA loaded Mt samples showed a general hydrophobicity increase, while for ODTMA loaded Na-Mica-4 samples constant hydrophobicity (CA values) from the external surface confirmed a low surfactant presence (Table 2), as was indicated by zeta potential measurements.

For ODA loaded samples (Mt and Na-Mica-4), the TSSA values were again directly related to the organic content (Fig. 4), as for ODTMA loaded samples. However, although CA values showed a hydrophobicity increase with the presence of this surfactant in around 40% of CEC (Tables 1 and 2), higher ODA loading (76.4% CEC) produced a subsequent decrease in CA values. These effects on TSSA and CA values indicated a different hydrophilicity/hydrophobicity behavior on the total and external surfaces of both samples with ODA loading.

It is important to note that the difference of TSSA values between both ODA-Mt samples (136 m^2/g) is greater than that for ODA-mica samples (16 m^2/g),

while for CA values these differences remained constant (10 °). These effects were associated with the lower amount of ODA present in the ODA-Mt than in ODA-Mica-4 samples (mass loss percentage in Tables 1 and 2), which were not reflected by the % CEC loaded value comparison between them due to the different Mt and Na-Mica-4 CEC´s. The presence of ODA molecules mostly on the internal rather than on the external surface of both samples, evidenced by the results of XRD and zeta potential (Fig. 1 and 3), was corroborated by the TSSA and CA differences found.

Summing up, the opposite change in the hydrophilicity/hydrophobicity behavior found within the ODTMA and ODA loaded samples indicates not only the different affinity, but also the different steric hindrance of the polar head of both surfactants with the solid surfaces, in agreement with that reported recently by Pesquera et al. [52] in organo-micas.

3.5. PRM Adsorption

A first approach to study PRM adsorption onto all clay samples was made by using a PRM solution at C_i = 80 mg/L (Fig. 5).

The different adsorption behaviors between raw Na-Mica-4 and Mt samples could be assigned to the acidic nature of Mt and also to the cationic exchange of PRM at the Mt interlayer as was found in previous work [75].

PRM adsorption attained 30% for Mt sample, and although the adsorption increased with the loading of both surfactants, for ODA it did not exceed 25%, while for ODTMA it reached 50%. The greater PRM retention for ODTMA than for ODA exchanged surfactant in Mt sample, despite the similar surfactant amount exchanged (Table 1), could be explained by more hydrophobic interactions between the organic fraction and the fungicide [75], which are generated by the higher polar head of ODTMA than ODA molecules. This behavior also explains the increase of PRM adsorption with the increase in the loading of both surfactants.

In Na-Mica-4 sample the PRM adsorption percentage was lower than 10%, and a general adsorption decrease was found for all surfactant exchanged samples. The similar PRM adsorption found for both ODTMA exchanged micas,

within the error values, could be related to the low ODTMA loaded/loading (Table 2). However, for ODA exchanged mica samples the slight PRM adsorption increase found with this surfactant amount loaded could be assigned to a freer external surface of the ODA-Mica-100 than ODA-Mica-50 samples, as shown by the zeta potential analysis (Fig. 3 D).

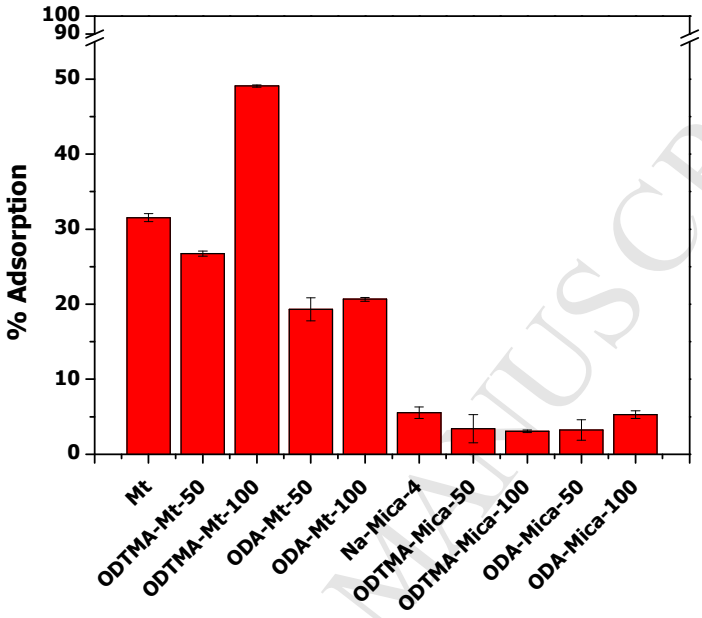

Fig. 5. PRM adsorption percentage of indicated samples.

4. CONCLUSIONS

XRD indicated similar arrangements of both surfactants in organo-Mt and organo-mica interlayer samples with a paraffin-like arrangement formed with the higher surfactant loading. However, in ODTMA-Mica-4 samples a partially free interlayer surface was found in addition to the paraffin-like arrangement. Evaluation of surfactant loading amount by Tg analysis showed values of around 40% and 80% of the respective CEC for ODA-Mt and ODA-Mica-4 samples and also for ODTMA-Mt samples, while only 2.6% and 10.6% of CEC was found for ODTMA-Mica-4. The presence of both surfactants in the external surface of Mt was followed by changes in the surface electric charges, which increased the hydrophobic properties of the loaded products. However, in ODTMA-Mica-4 samples, the behavior of surface electric charges indicated the presence of particles as a mixture of surfactant ion pairs and clay, despite attaining a hydrophobic behavior greater than that of Na-Mica-4 sample. In ODA-Mica-4 samples, different effects were related to the actual surfactant

loading. At low ODA loading, a slight decrease of surface negative electric charge was found, while at high ODA loading, the surfactant was released into the solution.

For ODTMA loaded samples a hydrophobicity increase with the surfactant content was found, while ODA loading increase generated an opposite behavior in CA and TSSA values, which indicated the presence of ODA molecules mostly on the internal rather than on the external surface of both samples.

The more acidic nature of Mt than Na-Mica-4 sample and the existence of PRM cationic exchange in Mt could be responsible for the PRM adsorption differences found in these samples. The higher PRM adsorption increase with ODTMA than ODA surfactants loaded in Mt sample could be explained by more hydrophobic interactions between the organic fraction and the fungicide when quaternary ammonium was employed. However, for Na-Mica-4 exchanged samples the PRM adsorption decrease with respect to the initial Na-Mica-4 sample was assigned to the low surfactant amount for ODTMA loaded samples, and for ODA exchanged samples a freer outer surface with ODA increase could be responsible for the slight PRM adsorption increase found.

Acknowledgements

Financial support from the Argentine Ministry of Science, Technology and Innovation - FONARSEC FS-Nano 008 is gratefully acknowledged. R.M. Torres and G. Curutchet are members of the National Council of Scientific and Technological Research (CONICET), and F.M. Flores and C. Fernández acknowledge CONICET fellowships. We gratefully acknowledge the support of the X-ray Laboratory of the Innovation, Technology and Research Center of Sevilla University (CITIUS), and of Seville University (through the VI Plan Propio de Investigación) for the mobility grant awarded to M.M. Orta in CETMIC (CONICET).

Appendix A. Supplementary material

REFERENCES

[1] Y.D. Noh, S. Komarneni, Mercury(II) Exchange by Highly Charged Swelling Micas, Sodium Engelhard Titanosilicate-4, and Sodium Titanosilicate, Environ. Sci. Technol., 45 (2011) 6954-6960. https://doi.org/10.1021/es200712r.
[2] A.P. Magnoli, L. Tallone, C.A.R. Rosa, A.M. Dalcero, S.M. Chiacchiera, R.M. Torres Sanchez, Commercial bentonites as detoxifier of broiler feed contaminated with aflatoxin, Appl. Surf. Sci., 40 (2008) 63-71. https://doi.org/10.1016/j.clay.2007.07.007.
[3] M. Park, D.H. Lee, C.L. Choi, S.S. Kim, K.S. Kim, J. Choi, Pure Na-4-mica: Synthesis and characterization, Chem. Mater., 14 (2002) 2582-2589. https://doi.org/10.1021/cm0116267.
[4] M.D. Alba, M.A. Castro, M. Naranjo, E. Pavón, Hydrothermal reactivity of Na-n-micas (n = 2, 3, 4), Chem. Mater., 18 (2006) 2867-2872. https://doi.org/10.1021/cm0514802.
[5] S. Komarneni, R. Ravella, Novel clays: Solid-state synthesis, characterization and cation exchange selectivity, Curr. Appl. Phys., 8 (2008) 104-106. https://doi.org/10.1016/j.cap.2007.04.012.
[6] K.G. Bhattacharyya, S.S. Gupta, Adsorption of a few heavy metals on natural and modified kaolinite and montmorillonite: a review, Adv. Colloid. Interfac., 140 (2008) 114-131.
[7] S.S. Gupta, K.G. Bhattacharyya, Kinetics of adsorption of metal ions on inorganic materials: a review, Adv. Colloid. Interfac., 162 (2011) 39-58.
[8] C. Maqueda, M. Dos Santos Afonso, E. Morillo, R.M. Torres Sánchez, M. Perez-Sayago, T. Undabeytia, Adsorption of diuron on mechanically and thermally treated montmorillonite and sepiolite, App. Clay Sci., 72 (2013) 175-183. https://doi.org/10.1016/j.clay.2012.10.017.
[9] J.L. Marco-Brown, M.M. Areco, R.M. Torres Sánchez, M. Dos Santos Afonso, Adsorption of picloram herbicide on montmorillonite: Kinetic and equilibrium studies, Colloid. Surface. A, 449 (2014) 121-128. https://doi.org/10.1016/j.colsurfa.2014.02.038.
[10] J. Madejová, H. Pálková, Ľ. Jankovič, Degradation of surfactant-modified montmorillonites in HCl, Mat. Chem. Phys., 134 (2012) 768-776. https://doi.org/10.1016/j.matchemphys.2012.03.067.
[11] Y. Xi, R.L. Frost, H. He, Modification of the surfaces of Wyoming montmorillonite by the cationic surfactants alkyl trimethyl, dialkyl dimethyl, and trialkyl methyl ammonium bromides, J. Colloid Interface Sci., 305 (2007) 150-158. https://doi.org/10.1016/j.jcis.2006.09.033.
[12] A.E. Bianchi, M. Fernández, M. Pantanetti, R. Viña, I. Torriani, R.M. Torres Sánchez, G. Punte, ODTMA+ and HDTMA+ organo-montmorillonites characterization: New insight by WAXS, SAXS and surface charge, App. Clay Sci., 83-84 (2013) 280-285. https://doi.org/10.1016/j.clay.2013.08.032.
[13] S. Yamagata, Y. Hamba, T. Akasaka, N. Ushijima, M. Uo, J. Iida, F. Watari, The effect of enhancing the hydrophobicity of OMMT on the characteristics of PMMA/OMMT nanocomposites, Appl. Surf. Sci., 262 (2012) 56-59. https://doi.org/10.1016/j.apsusc.2012.01.081.
[14] P. Huang, A. Kazlauciunas, R. Menzel, L. Lin, Determining the mechanism and efficiency of industrial dye adsorption through facile structural control of organo-montmorillonite adsorbents, ACS Appl. Mater. Inter., 9 (2017) 26383-26391.
[15] R. Hojiyev, G. Ersever, T.E. Karaağaçlioğlu, F. Karakaş, F. Boylu, Changes on montmorillonite characteristics through modification, Appl. Clay Sci., 127-128 (2016) 105-110. https://doi.org/10.1016/j.clay.2016.03.042.
[16] J. Lee, H. Lee, Characterization of organobentonite used for polymer nanocomposites, Mat. Chem. Phys., 85 (2004) 410-415. https://doi.org/10.1016/j.matchemphys.2004.01.032.
[17] R. Song, Z. Wang, X. Meng, B. Zhang, T. Tang, Influences of catalysis and dispersion of organically modified montmorillonite on flame retardancy of polypropylene

nanocomposites, J. Appl. Polym. Sci., 106 (2007) 3488-3494. https://doi.org/10.1002/app.27033.
[18] Z. Huang, Y. Li, W. Chen, J. Shi, N. Zhang, X. Wang, Z. Li, L. Gao, Y. Zhang, Modified bentonite adsorption of organic pollutants of dye wastewater, Mater. Chem. Phys., 202 (2017) 266-276. https://doi.org/10.1016/j.matchemphys.2017.09.028.
[19] C. Breen, R. Watson, Acid-activated organoclays: preparation, characterisation and catalytic activity of polycation-treated bentonites, Appl. Clay Sci., 12 (1998) 479-494. https://doi.org/10.1016/s0169-1317(98)00006-4.
[20] I.M.C. Lo, R.K.M. Mak, S.C.H. Lee, Modified clays for waste containment and pollutant attenuation, J. Environ. Eng., 123 (1997) 25-32. https://doi.org/10.1061/(asce)0733-9372(1997)123:1(25).
[21] S.H. Lin, M.J. Cheng, Adsorption of phenol and m-chlorophenol on organobentonites and repeated thermal regeneration, Waste Manage., 22 (2002) 595-603. https://doi.org/10.1016/s0956-053x(01)00029-0.
[22] D. Doyle, A. Brown, Produced water treatment and hydrocarbon removal with organoclay, SPE Annual Technical Conference and Exhibition, Society of Petroleum Engineers, 2000.
[23] C.C. Santiago, M.A. Fernández, R.M. Torres Sánchez, Adsorption and characterization of MCPA on DDTMA- and raw-montmorillonite: Surface sites involved, J. Environ. Sci. Healt. B, 51 (2016) 245-253. https://doi.org/10.1080/03601234.2015.1120618.
[24] F.M. Flores, E.L. Loveira, F. Yarza, R. Candal, R.M. Torres Sánchez, Benzalkonium Chloride Surface Adsorption and Release by Two Montmorillonites and Their Modified Organomontmorillonites, Water Air Soil Poll., 228 (2017). https://doi.org/10.1007/s11270-016-3223-2.
[25] M. Gamba, M. Olivelli, J.M. Lázaro-Martínez, G. Gaddi, G. Curutchet, R.M. Torres Sánchez, Thiabendazole adsorption on montmorillonite, octadecyltrimethylammonium- and Acremonium sp.-loaded products and their copper complexes, Chem. Eng. J., 320 (2017) 11-21. https://doi.org/10.1016/j.cej.2017.03.034.
[26] M.C. Pazos, M.A. Castro, A. Cota, F.J. Osuna, E. Pavón, M.D. Alba, New insights into surface-functionalized swelling high charged micas: Their adsorption performance for non-ionic organic pollutants, J. Ind. Eng. Chem., 52 (2017) 179-186. https://doi.org/10.1016/j.jiec.2017.03.042.
[27] M.D.M. Orta, J. Martín, S. Medina-Carrasco, J.L. Santos, I. Aparicio, E. Alonso, Novel synthetic clays for the adsorption of surfactants from aqueous media, J. Environ. Manage., 206 (2018) 357-363. https://doi.org/10.1016/j.jenvman.2017.10.053.
[28] J.J. Smoot, L.G. Houck, H.B. Johnson, Market diseases of citrus and other sub-tropical fruits, USDA, ARS, USA, 1971.
[29] M. Komárek, E. Čadková, V. Chrastný, F. Bordas, J.C. Bollinger, Contamination of vineyard soils with fungicides: A review of environmental and toxicological aspects, Environ. Int., 36 (2010) 138-151. https://doi.org/10.1016/j.envint.2009.10.005.
[30] R. Caiazzo, Y.K. Kim, C.L. Xiao, Occurrence and phenotypes of pyrimethanil resistance in Penicillium expansum from apple in Washington State, Plant Dis., 98 (2014) 924-928. https://doi.org/10.1094/pdis-07-13-0721-re.
[31] P. Cabras, A. Angioni, Pesticide residues in grapes, wine, and their processing products, J. Agr. Food Chem., 48 (2000) 967-973. https://doi.org/10.1021/jf990727a.
[32] (EPA), General overview: Reduced risk pesticide program, Environmental Protection Agency, Environ. Prot. Agency Off. Pestic. programs, 1998, pp. 2-4.
[33] M. Gamba, F.M. Flores, J. Madejová, R.M. Torres Sánchez, Comparison of imazalil removal onto montmorillonite and nanomontmorillonite and adsorption surface sites involved: An approach for agricultural wastewater treatment, Ind. Eng. Chem. Res., 54 (2015) 1529-1538. https://doi.org/10.1021/ie5035804.

[34] M.D. Alba, M.A. Castro, M.M. Orta, E. Pavón, M.C. Pazos, J.S. Valencia Rios, Formation of organo-highly charged mica, Langmuir, 27 (2011) 9711-9718. https://doi.org/10.1021/la200942u.
[35] D. Wang, Theoretical Criteria and Calculation for Collector Performance, Flotation Reagents: Applied Surface Chemistry on Minerals Flotation and Energy Resources Beneficiation, Springer, Singapore, 2016, pp. 135-277.
[36] M.J. Rosen, J.T. Kunjappu, Surfactants and interfacial phenomena, 4th ed., John Wiley & Sons, New Jersey, 2012.
[37] PPDB:, Pesticide Properties Data Base, University of Hertfordshire, Hatfield, Hertfordshire, UK, 2011.
[38] A.M. Fernández Solarte, J. Villarroel-Rocha, C. Fernández Morantes, M.L. Montes, G. Curutchet, K. Sapag, R.M. Torres Sánchez, Insight into surface and structural changes of montmorillonite and organo-montmorillonites loaded with Ag, (2019) CRAS2C_4556_edit_report.
[39] P. Huang, A. Kazlauciunas, R. Menzel, L. Lin, Determining the Mechanism and Efficiency of Industrial Dye Adsorption through Facile Structural Control of Organo-montmorillonite Adsorbents, ACS Appl. Mater. Interfaces, 9 (2017) 26383-26391. https://doi.org/10.1021/acsami.7b08406.
[40] W. Xie, Z. Gao, W.P. Pan, D. Hunter, A. Singh, R. Vaia, Thermal degradation chemistry of alkyl quaternary ammonium Montmorillonite, Chem. Mater., 13 (2001) 2979-2990. https://doi.org/10.1021/cm010305s.
[41] E.M. Pecini, M.J. Avena, Measuring the isoelectric point of the edges of clay mineral particles: The case of montmorillonite, Langmuir, 29 (2013) 14926-14934. https://doi.org/10.1021/la403384g.
[42] R.M. Torres Sánchez, S. Falasca, Specific surface area and surface charges of some argentinian soils, J. Plant Nutr. Soil Sci., 160 (1997) 223-226.
[43] A. Metya, D. Ghose, N.R. Ray, Development of hydrophobicity of mica surfaces by ion beam sputtering, Appl. Surf. Sci., 293 (2014) 18-23. https://doi.org/10.1016/j.apsusc.2013.11.163.
[44] C. Peng, F. Min, L. Liu, Effect of pH on the adsorption of dodecylamine on montmorillonite: Insights from experiments and molecular dynamics simulations, Appl. Surf. Sci., 425 (2017) 996-1005. https://doi.org/10.1016/j.apsusc.2017.07.085.
[45] A.F. Stalder, T. Melchior, M. Müller, D. Sage, T. Blu, M. Unser, Low-bond axisymmetric drop shape analysis for surface tension and contact angle measurements of sessile drops, Colloid. Surface. A, 364 (2010) 72-81. https://doi.org/10.1016/j.colsurfa.2010.04.040.
[46] W. Rasband, WS 1997-2012. ImageJ, US National Institutes of Health, Bethesda, Maryland, USA, 2012.
[47] T. Iwasaki, T. Watanabe, Distribution of Ca and Na ions in dioctahedral smectites and interstratified dioctahedral mica/smectites, Clays Clay Miner., 36 (1988) 73-82. https://doi.org/10.1346/CCMN.1988.0360110.
[48] Z. Klapyta, T. Fujita, N. Iyi, Adsorption of dodecyl- and octadecyltrimethylammonium ions on a smectite and synthetic micas, Appl. Clay Sci., 19 (2001) 5-10. https://doi.org/10.1016/s0169-1317(01)00059-x.
[49] B. Schampera, D. Tunega, R. Šolc, S.K. Woche, R. Mikutta, R. Wirth, S. Dultz, G. Guggenberger, External surface structure of organoclays analyzed by transmission electron microscopy and X-ray photoelectron spectroscopy in combination with molecular dynamics simulations, J. Colloid Interf. Sci., 478 (2016) 188-200. https://doi.org/10.1016/j.jcis.2016.06.008.
[50] M.C. Pazos, M.A. Castro, M.M. Orta, E. Pavón, J.S.V. Rios, M.D. Alba, Synthetic high-charge organomica: Effect of the layer charge and alkyl chain length on the structure of the adsorbed surfactants, Langmuir, 28 (2012) 7325-7332. https://doi.org/10.1021/la300153e.

[51] K. Tamura, H. Nakazawa, Intercalation of N-alkyltrimethylammonium into swelling fluoro-mica, Clays Clay Miner., 44 (1996) 501-505. https://doi.org/10.1346/CCMN.1996.0440408.
[52] C. Pesquera, F. Aguado, F. González, C. Blanco, L. Rodríguez, A.C. Perdigón, Tunable interlayer hydrophobicity in a nanostructured high charge organo-mica, Micropor. Mesopor. Mat., 263 (2018) 77-85. https://doi.org/10.1016/j.micromeso.2017.12.006.
[53] S. Komarneni, A.R. Aref, S. Hong, Y.D. Noh, F.S. Cannon, Y. Wang, Organoclays of high-charge synthetic clays and alumina pillared natural clays: Perchlorate uptake, Appl. Clay Sci., 80-81 (2013) 340-345. https://doi.org/10.1016/j.clay.2013.06.001.
[54] C.B. Hedley, G. Yuan, B.K.G. Theng, Thermal analysis of montmorillonites modified with quaternary phosphonium and ammonium surfactants, Appl. Clay Sci., 35 (2007) 180-188. https://doi.org/10.1016/j.clay.2006.09.005.
[55] S. Xu, S.A. Boyd, Cationic surfactant adsorption by swelling and nonswelling layer silicates, Langmuir, 11 (1995) 2508-2514. https://doi.org/10.1021/la00007a033.
[56] R. Liu, R.L. Frost, W.N. Martens, Y. Yuan, Synthesis, characterization of mono, di and tri alkyl surfactant intercalated Wyoming montmorillonite for the removal of phenol from aqueous systems, J. Colloid Interf. Sci., 327 (2008) 287-294. https://doi.org/10.1016/j.jcis.2008.08.049.
[57] L. Le Pluart, J. Duchet, H. Sautereau, J.F. Gérard, Surface modifications of montmorillonite for tailored interfaces in nanocomposites, J. Adhes., 78 (2002) 645-662. https://doi.org/10.1080/00218460213738.
[58] C.T. Cowan, D. White, The mechanism of exchange reactions occurring between sodium montmorillonite and various n-primary aliphatic amine salts, T. Faraday Soc., 54 (1958) 691-697. https://doi.org/10.1039/tf9585400691.
[59] G. Morozov, V. Breus, S. Nekludov, I. Breus, Sorption of volatile organic compounds and their mixtures on montmorillonite at different humidity, Colloid. Surface. A, 454 (2014) 159-171. https://doi.org/10.1016/j.colsurfa.2014.03.104.
[60] M.D. Alba, M.A. Castro, M. Naranjo, M.M. Orta, E. Pavón, M.C. Pazos, Evolution of phases and Al-Si distribution during Na-4-mica synthesis, J. Phys. Chem. C, 115 (2011) 20084-20090. https://doi.org/10.1021/jp207408h.
[61] S. Yariv, The role of charcoal on DTA curves of organo-clay complexes: An overview, Appl. Clay Sci., 24 (2004) 225-236. https://doi.org/10.1016/j.clay.2003.04.002.
[62] F. Thomas, L.J. Michot, D. Vantelon, E. Montargès, B. Prélot, M. Cruchaudet, J.F. Delon, Layer charge and electrophoretic mobility of smectites, Colloid. Surface. A, 159 (1999) 351-358. https://doi.org/10.1016/s0927-7757(99)00291-5.
[63] B.M. Lombardi, R.M. Torres Sanchez, P. Eloy, M. Genet, Interaction of thiabendazole and benzimidazole with montmorillonite, App. Clay Sci., 33 (2006) 59-65. https://doi.org/10.1016/j.clay.2006.03.010.
[64] O. Cubuk, B. Caglar, C. Topcu, F. Coldur, G. Sarp, A. Tabak, E. Sahin, Structural characterization of hexadecyltrimethylammonium-smectite composites and their potentiometric electrode applications, Appl. Surf. Sci., 338 (2015) 99-112. https://doi.org/10.1016/j.apsusc.2015.02.110.
[65] P. Praus, M. Turicová, S. Študentová, M. Ritz, Study of cetyltrimethylammonium and cetylpyridinium adsorption on montmorillonite, J. Colloid Interf. Sci., 304 (2006) 29-36. https://doi.org/10.1016/j.jcis.2006.08.038.
[66] H. Heinz, R.A. Vaia, R. Krishnamoorti, B.L. Farmer, Self-assembly of alkylammonium chains on montmorillonite: Effect of chain length, head group structure, and cation exchange capacity, Chem. Mater., 19 (2007) 59-68. https://doi.org/10.1021/cm062019s.
[67] T.H. Wang, C.J. Hsieh, S.M. Lin, D.C. Wu, M.H. Li, S.P. Teng, Effect of alkyl properties and head groups of cationic surfactants on retention of cesium by

organoclays, Environ. Sci. Technol., 44 (2010) 5142-5147. https://doi.org/10.1021/es100349k.
[68] R.M. Pashley, Electromobility of mica particles dispersed in aqueous solutions, Clay. Clay Miner., 33 (1985) 193-199. https://doi.org/10.1346/CCMN.1985.0330304.
[69] C. Taubaso, M. Dos Santos Afonso, R.M. Torres Sánchez, Modelling soil surface charge density using mineral composition, Geoderma, 121 (2004) 123-133. https://doi.org/10.1016/j.geoderma.2003.11.005.
[70] M. Tschapek, R.M. Torres Sanchez, C. Wasowski, PZC of Al2O3 + SiO2 mixtures, Anales de edafología y agrobiología., 38 (1979) 589-594.
[71] B. Caglar, B. Afsin, A. Tabak, E. Eren, Characterization of the cation-exchanged bentonites by XRPD, ATR, DTA/TG analyses and BET measurement, Chem. Eng. J., 149 (2009) 242-248. https://doi.org/10.1016/j.cej.2008.10.028.
[72] R.M. Torres Sánchez, M.J. Genet, E.M. Gaigneaux, M. dos Santos Afonso, S. Yunes, Benzimidazole adsorption on the external and interlayer surfaces of raw and treated montmorillonite, App. Clay Sci., 53 (2011) 366-373. https://doi.org/10.1016/j.clay.2010.06.026.
[73] F. Barraqué, M.L. Montes, M.A. Fernández, R.C. Mercader, R.J. Candal, R.M. Torres Sánchez, Synthesis and characterization of magnetic-montmorillonite and magnetic-organo-montmorillonite: Surface sites involved on cobalt sorption, J Magn Magn Mater, 466 (2018) 376-384. https://doi.org/10.1016/j.jmmm.2018.07.052.
[74] L. Lorenzo, E.F. Torres, P. Naranjo, R.T. Sánchez, Adsorción de As en 4-Na-Mica sintética y su producto de tratamiento mecánico, in: M. Blesa, M.D.S. Afonso, R.M.T. Sánchez (Eds.) Las fronteras de la Física y la química ambiental en Ibero América, Universidad Nacional de San Martín, Buenos Aires, Argentina, 2008, pp. 314-319.
[75] F.M. Flores, T. Undabeytia, E. Morillo, R.M. Torres Sánchez, Technological applications of organo-montmorillonites in the removal of pyrimethanil from water: adsorption/desorption and flocculation studies, Environ. Sci. Pollut. R., (2017) 1-14. https://doi.org/10.1007/s11356-017-9016-3.

Figure Captions

Fig. 1. XRD patterns of (A) Mt and (B) Na-Mica-4 and the respective ODA / ODTMA loaded samples. Insets: deconvolution of 001 peak for indicated samples.

Fig. 2. Derivative plot of thermal degradation (DTg) for A) Mt and ODTMA / ODA loaded Mt samples, and B) Na-Mica-4 and ODTMA / ODA loaded mica samples.

Fig. 3. Zeta potential versus pH curves for (A) (■) Mt, (▼) ODTMA-Mt-50 and (▲) ODTMA-Mt-100; (B) (■) Mt, (◀) ODA-Mt-50, (▶) and ODA-Mt-100; (C) (○) Na-Mica-4, (▽) ODTMA-Mica-50, and (△) ODTMA-Mica-100; and (D) (○) Na-Mica-4, (◁) ODA- Mica-50, and (▷)ODA-Mica-100 samples.

Fig. 4. 3D plot of % CEC, TSSA and CA values for: (A) (■) Mt, (▼) ODTMA-Mt-50 and (▲) ODTMA-Mt-100, (◀) ODA-Mt-50, (▶) and ODA-Mt-100; (B) (○) Na-Mica-4, (▽) ODTMA-Mica-50, and (△) ODTMA-Mica-100, (◁) ODA- Mica-50, and (▷)ODA-Mica-100 samples. The CEC value of raw samples (Mt and Na-Mica-4 samples) was taken as zero in order to compare TSSA and CA values with the % CEC increase of the respective surfactant loaded. The dotted lines indicate the point projections to the ZX and ZY planes.

Fig. 5. PRM adsorption percentage of indicated samples.

Table of Contents/Abstract Graphic

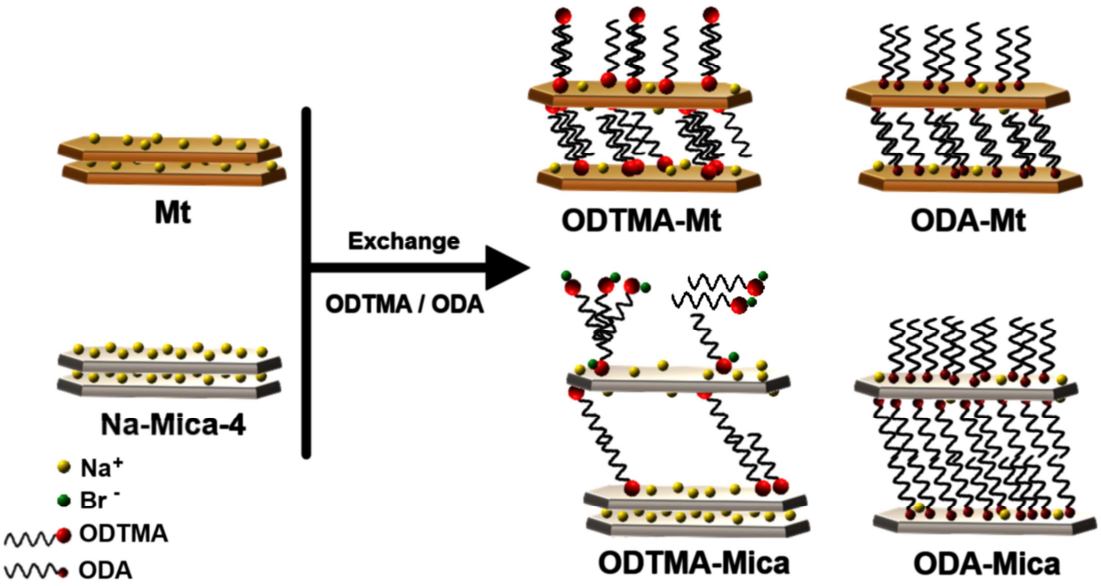

Highlights

- Raw Mt and synthetic mica were exchanged with primary and quaternary alkylammonium.
- A partial free interlayer surface was found in ODTMA-Mica-4 samples.
- The zeta potential indicated mixture of surfactant ion pairs and clay in ODTMA-Mica-4 samples.
- Hydrophobicity in both organo-clay increased with the ODTMA content.
- The low PRM adsorption in organo-mica samples was related to surfactant freer outer surface.